Cerebral Cortex January 2011;21:233–244
doi:10.1093/cercor/bhq090
Advance Access publication May 19, 2010

Cerebral Blood Flow in Posterior Cortical Nodes of the Default Mode Network Decreases with Task Engagement but Remains Higher than in Most Brain Regions

Adolf Pfefferbaum[1,2], Sandra Chanraud[1,2], Anne-Lise Pitel[2], Eva Müller-Oehring[1,2], Ajit Shankaranarayanan[3], David C. Alsop[4], Torsten Rohlfing[1] and Edith V. Sullivan[2]

[1]Neuroscience Program, SRI International, Menlo Park, CA 94025, USA, [2]Department of Psychiatry and Behavioral Sciences, Stanford University School of Medicine, Stanford, CA 94305, USA, [3]MR Applied Systems Laboratory, General Electric Healthcare, Menlo Park, CA 94025, USA and [4]Department of Radiology, Beth Israel Deaconess Medical Center and Harvard Medical School, Boston, MA 02215, USA

Address correspondence to Edith V. Sullivan, PhD, Department of Psychiatry and Behavioral Sciences, Stanford University School of Medicine, 401 Quarry Road, Stanford, CA 94305-5723, USA. Email: edie@stanford.edu.

Functional neuroimaging studies provide converging evidence for existence of intrinsic brain networks activated during resting states and deactivated with selective cognitive demands. Whether task-related deactivation of the default mode network signifies depressed activity relative to the remaining brain or simply lower activity relative to its resting state remains controversial. We employed 3D arterial spin labeling imaging to examine regional cerebral blood flow (CBF) during rest, a spatial working memory task, and a second rest. Change in regional CBF from rest to task showed significant normalized and absolute CBF reductions in posterior cingulate, posterior-inferior precuneus, and medial frontal lobes . A Statistical Parametric Mapping connectivity analysis, with an a priori seed in the posterior cingulate cortex, produced deactivation connectivity patterns consistent with the classic "default mode network" and activation connectivity anatomically consistent with engagement in visuospatial tasks. The large task-related CBF decrease in posterior-inferior precuneus relative to its anterior and middle portions adds evidence for the precuneus' heterogeneity. The posterior cingulate and posterior-inferior precuneus were also regions of the highest CBF at rest and during task performance. The difference in regional CBF between intrinsic (resting) and evoked (task) activity levels may represent functional readiness or reserve vulnerable to diminution by conditions affecting perfusion.

Keywords: ASL, cerebral blood flow, cingulate, default mode network, precuneus

Introduction

Nonactivated, resting state functional neuroimaging studies provide converging evidence for the existence of intrinsically connected brain networks. These resting state networks are considered pertinent as antecedent states to specific cognitive functions, such as executive control and salience detection (Seeley et al. 2007; Buckner et al. 2008; Krienen and Buckner 2009). Of special prominence is the "default mode network," comprising the posterior cingulate cortex, precuneus, inferior parietal cortex, medial prefrontal cortex (Shulman et al. 1997; Mazoyer et al. 2001; Raichle et al. 2001; Greicius et al. 2003, 2004), and also the medial temporal lobe (Greicius et al. 2004; Andrews-Hanna et al. 2010; cf. Minoshima et al. 1997). Activity of this network is considered to be a fundamental "intrinsic" aspect of brain functioning and has been posited to be a component of consciousness, sense of self, self-referential processing, and episodic memory (Raichle et al. 2001; Vincent et al. 2006; Buckner et al. 2008). First noted as regions of decreased blood oxygenation level–dependent (BOLD) activity when subjects engaged in tasks compared with nontask conditions (Shulman et al. 1997; Raichle et al. 2001), intrinsic networks are also demonstrable with BOLD in the "resting state" (Fox et al. 2009). During a resting state, nodes of the default network have higher correlated intrinsic low-frequency BOLD signal (Greicius et al. 2009) or regional cerebral blood flow (CBF) (Zou et al. 2009) among themselves than with other brain structures. With engagement in selective tasks, such as working memory or visuospatial problem solving (Buckner et al. 2008) but not cognitively simple sensory processing tasks (Greicius et al. 2003), this network is "deactivated" (Raichle et al. 2001). Deactivation with task demands, however, may not necessarily indicate that the nodes of this network are inactive. Indeed, microelectrode unit recordings in cingulate, limbic, insular, and entorhinal cortices in the cat during waking and sleeping revealed a complex relationship between task-positive and resting-state networks; associated with decreased local field potentials was an increased cell firing rate in the same network, suggesting enhanced rather than reduced activity with attentional demands in a task-off brain region (Popa et al. 2009). Whether task-related deactivation of the default mode network in humans signifies depressed activity relative to the remaining brain or simply lower activity relative to its resting state level yet equal to or higher than other brain regions, remains controversial. Determination of which of these possibilities characterizes the switch from intrinsic to evoked activity of the default mode network requires absolute quantification of regional brain activity in the context of a rest versus cognitive challenge experiment.

Neural activity associated with cognitive demands is mediated by complex interactions between neurons, glial cells, and vascular smooth muscle cells (D'Esposito et al. 2003) and marked by changes in CBF local to regions involved in meeting task demands (Leniger-Follert and Hossmann 1977). Thus, fluctuations in CBF can provide contrast between an active brain region and surrounding resting tissue (Kelly et al. 2010) and serve to localize brain regions that comprise a functional network (e.g., Raichle and Snyder 2007). Activation imaging using arterial spin labeling (ASL) yields quantitative maps of CBF (Detre et al. 1992), eliminating the necessity to compare a target with a referent condition (Buxton et al. 1998; Wong et al. 1998). High reliability (e.g., Aguirre et al. 2002; Wang et al. 2003; Parkes et al. 2004; MacIntosh et al. 2008; Petersen et al. 2010; Pfefferbaum et al. 2010; Xu et al. 2010) makes the potential of activated CBF attractive for clinical and longitudinal studies. A primary advantage of activation ASL imaging is

that the signal is directly related to blood flow and, like positron emission tomography (PET) (Raichle et al. 2001), can provide quantitative and absolute measurements of CBF in different brain regions reflecting their level of activity.

Initial ASL activation studies used tasks with low demands, such as passive visual stimulation (Talagala and Noll 1998; Aguirre et al. 2002) and memory-guided sequential finger movement task (Garraux et al. 2005) but were successful in causing increases in several task-relevant areas of perfusion (e.g., left primary motor cortex and dorsal lateral premotor cortices) and decreases in others (e.g., right posterior cingulate gyrus). Relative to rest, finger tapping consistently modulated the somatosensory motor cortex bilaterally even when rest and the task were separated by one day (Wang et al. 2003). A few studies employing tasks with higher cognitive demands used single slice imaging protocols, thereby limiting exploration of whole-brain activation patterns associated with the tasks (Ye et al. 2000; Mildner et al. 2005; Bangen et al. 2009). Studies using whole-brain CBF protocols have examined patterns of CBF changes during sustained attention and visual working memory in healthy subjects (Kim et al. 2006) and during memory encoding in patients with mild cognitive impairment (Xu et al. 2010) and have revealed substantial regional CBF differences, with some brain regions showing increased CBF and others decreased CBF, when task blocks were compared with rest blocks. Lim et al. (2009) compared pretask rest and post-task rest blocks and showed decreased CBF in a fronto–parietal network during the post-task rest compared with the pretask block that was interpreted as persistent cognitive fatigue. The posterior cingulate cortex and precuneus had significantly decreased CBF (deactivation) in task relative to rest blocks.

Brain regions consistently exhibiting high CBF (i.e., activation) during a resting state and lower CBF (i.e., deactivation) during a task are the posterior cingulate cortex, precuneus, and medial prefrontal cortex (Greicius et al. 2003; Fransson and Marrelec 2008; Damoiseaux and Greicius 2009; Detre et al. 2009; for reviews, Raichle 2009). PET studies based either on the oxygen extraction fraction (Raichle et al. 2001) or on the regional CBF (Mazoyer et al. 2001) have identified specific brain regions with high activity during rest relative to demanding tasks when these regions have lower activity. Functional connectivity magnetic resonance imaging (fcMRI) using BOLD signal fluctuations and low-frequency intrinsic functional correlations enabled identification of networks of brain regions with high connectivity during resting conditions (Greicius et al. 2003; Andrews-Hanna et al. 2010). These core regions of the default mode network have been speculated to enable self-related mental processing (Shulman et al. 1997; Mazoyer et al. 2001; Raichle et al. 2001; Buckner et al. 2008; Andrews-Hanna et al. 2010) through intrinsic brain activity (Fransson 2006; Fransson and Marrelec 2008). Comparison of intrinsic and evoked activity may provide insight as to how the intrinsic mode modulates goal-directed task performance (cf. Raichle and Gusnard 2005).

Here, we combined whole-brain pulsed continuous ASL (PCASL) imaging (Dai et al. 2008) with high-resolution parcellated structural MRI to quantify changes in regional CBF during performance of a cognitive task involving spatial working memory and during rest blocks before and after the task. We tested the hypothesis that regional CBF would be influenced by task demands and that regions associated with the default mode network, particularly the posterior cingulate, precuneus, and medial frontal cortices, would be diminished during task engagement, while other cortical or subcortical regions would be activated relative to their resting state. Furthermore, we predicted that the posterior–inferior division of the precuneus would be the main source of CBF task-related variation (cf. Margulies et al. 2009; Pfefferbaum et al. 2010). In keeping with the functional MRI literature, we refer to enhanced CBF as "activation" and diminished CBF as "deactivation." Accordingly, we examined CBF changes related to task demands with parcellated whole-brain analyses to obtain specific measures in each cortical, subcortical, and cerebellar region. In addition to using a region-of-interest (ROI) analysis, we calculated whole-brain temporal connectivity maps across the 3 experimental conditions of Rest 1, Task, and Rest 2 (cf. Chuang et al. 2008; Lim et al. 2009; Zou et al. 2009).

Materials and Methods

Subjects

The subjects were 6 men and 8 women, age 25 to 42 (mean = 31.4) years. All were highly educated (college graduates or beyond). None smoked cigarettes, and all were right handed as determined by quantitative testing (Crovitz and Zener 1962). None was permitted to have caffeinated beverages within an hour of the scanning session. Data were collected in a single session. All subjects provided written consent to participate in this study.

Image Acquisition

Data were collected on a GE 3T Signa Excite human whole-body system with a receive-only 8-channel array head coil and body transmit coil. The imaging protocol comprised 3 acquisitions of a whole-brain PCASL 3D perfusion sequence (Wang et al. 2005; Dai et al. 2008) (time repetition [TR] = 4.3 s, time echo [TE] = 10.1 ms, thick = 5 mm, skip = 0 mm, xy matrix = 518 × 8 (spiral acquisition); flip angle = 155°, locations = 36, field of view [FOV] = 240 mm, labeling duration = 1.5 s, post labeling delay = 2 s; imaging time 6 min 49 s) (Fig. 1). The PCASL was collected first while resting (Rest 1), then while performing a spatial working memory task (Task), and finally while resting again (Rest 2). Descriptions of the Rest and Task conditions are presented in the Rest and Cognitive Task Condition section.

Structural data also acquired were spoiled gradient recalled (SPGR) (TR = 5.916 ms, TE = 1.92 ms, thick = 1.3 mm, skip = 0 mm, xy matrix = 256; flip angle = 15°, locations = 124, FOV = 240 mm) and dual-echo fast spin-echo (FSE) (TR = 5000 ms, TE = 12.248/97.984 ms, thick = 2.5 mm, skip = 0 mm, xy matrix = 256; flip angle = 90°, locations = 72, FOV = 240 mm).

CBF Quantification

Following the method of Jarnum et al. (2010), PCASL quantification was based on a 2-compartment model (Alsop et al. 1996) with finite labeling duration (Wang et al. 2005). Calculation of flow was based on the following equation

$$f = \frac{\lambda}{2\alpha T_{1b}\left(1 - e^{-\frac{\tau}{T_{1b}}}\right)} \frac{(S_{\text{ctrl}} - S_{\text{lbl}})\left(1 - e^{-\frac{t_{\text{sat}}}{T_{1g}}}\right)}{S_{\text{ref}}} e^{\frac{w}{T_{1b}}}$$

where f is the flow; S is the signal from the control, label, or reference image as determined by the subscript; T_{1b} is the T_1 of blood; T_{1g} is the T_1 of gray matter; α is the labeling efficiency; λ is the brain–blood partition coefficient; t_{sat} is the saturation time for proton density images (2 s); τ is the labeling duration (1.5 s); and w is the post-labeling delay (2 s). The assumed parameters were 1.2 s for T_{1g} and 1.6 s for T_{1b}, 0.6 for effective labeling efficiency (Garcia et al. 2005; Dai et al. 2008), and 0.9 for the brain–blood partition coefficient (Herscovitch and Raichle 1985). The quantification was implemented using the Interactive Data Language.

Image Processing

For each subject, an intensity bias field correction was first applied to the SPGR and FSE images (Likar et al. 2001). The bias-corrected early-

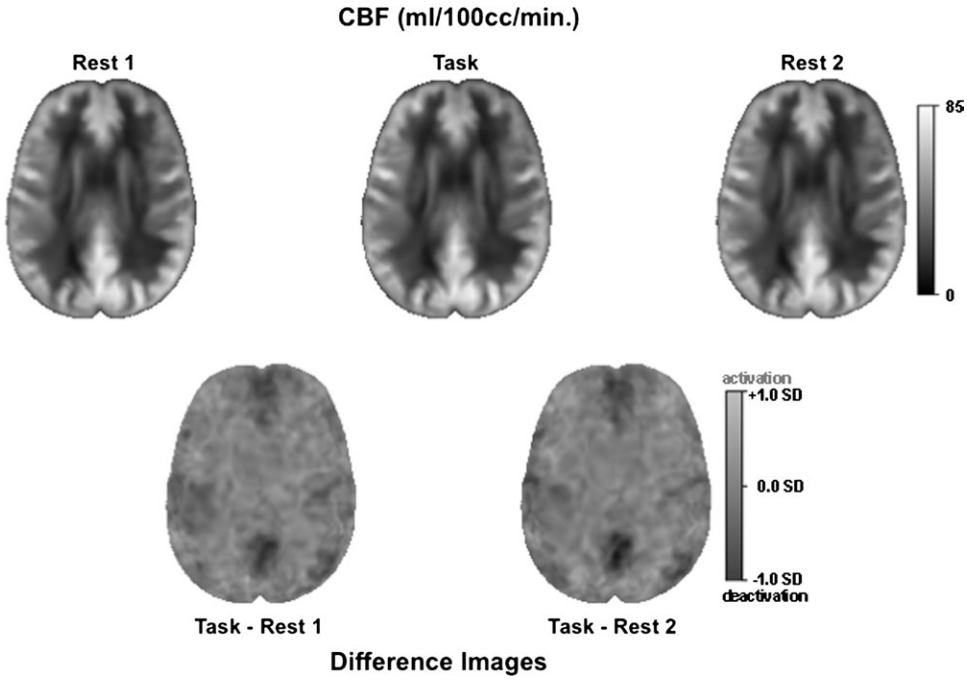

Figure 1. CBF images averaged across the 14 subjects. Top, left to right: example slices in the axial plane from each ASL condition: Rest 1, Task, and Rest 2. CBF is displayed as image intensity ranging from 0 to 85 mL/100cc/min. Bottom: examples of average difference CBF images at the same slice location as the single ASL condition above. Normalized difference in CBF is displayed as signal intensity ranging from deactivation (dark) to activation (bright) in SDs.

echo images were then aligned with the bias-corrected SPGR images via nonrigid registration (Rueckert et al. 1999; Rohlfing et al. 2003) (http://nitrc.org/projects/cmtk/). The early-echo and late-echo FSE images were acquired in alignment so that the early-echo-to-SPGR alignment also applied to the late-echo FSE image. Skull-stripped images were generated by running FSL BET (Smith 2002) on the SPGR, early-echo, and late-echo FSE images separately and combining the resulting brain masks by voting (Rohlfing and Maurer 2005) after reformatting the 2 FSE masks into SPGR space. The skull-stripped SPGR images were then segmented into 3 tissue classes (cerebrospinal fluid [CSF], gray matter; white matter) using FSL FAST (Zhang et al. 2001).

For each subject and each acquisition, the CBF images were aligned with the gray matter probability maps obtained from SPGR images using FAST. The rationale behind this procedure is that the CBF signal is expected to be predominantly in gray matter. We also evaluated other possible registration protocols using proton density-weighted images acquired in alignment with the CBF images as part of the ASL acquisition protocol. The tissue contrast and conspicuity of these auxiliary images were poor by visual inspection and resulted in unreliable and inaccurate registrations (Pfefferbaum et al. 2010).

Because the CBF value at each acquired pixel represents an estimate of an absolute physical quantity within the volume of that pixel, these values required correction for local volume changes when the CBF images were reformatted into the space of the structural images. To this end, the value of each reformatted interpolated CBF pixel was multiplied with the local Jacobian determinant of the nonrigid transformation from SPGR to CBF space, which represents the local volume change due to applying the deformation.

For ROI-based analysis and intersubject comparison, we registered all skull-stripped subject SPGR images to the SPGR channel of the SRI24 atlas (Rohlfing et al. 2010) (http://nitrc.org/projects/sri24/). Using these transformations, ROIs defined in the atlas were transferred to each subject's SPGR image space. The SRI24 atlas parcellation scheme, adapted from Tzourio-Mazoyer et al. (2002), was initially collapsed into 16 bilateral ROIs and a midline cerebellar vermis ROI (Table 1, from Pfefferbaum et al. 2010). Also, via concatenation of SRI24-to-subject with subject SPGR-to-subject CBF images, all CBF images were reformatted into SRI24 coordinate space for averaging and visualization. Again, reformatted CBF values had to be corrected for local volume changes, but we conceptually distinguished between the within-subject parts of the total transformation, for which we corrected the CBF images using local Jacobian determinants, and subject-to-atlas parts, for which no correction was applied.

Regional CBF Quantification

Using the segmentation maps in each subject's native space, data were analyzed as CBF in mL/100cc of gray matter/min for the cortical regions and total tissue for subcortical (hippocampus–amygdala, caudate–putamen, globus pallidus, and thalamus) and all cerebellar regions. For the primary regional analysis for each condition, the CBF data were corrected for interindividual variations in global CBF and expressed as globally normalized data (i.e., standardized or *Z*-scores) by dividing the CBF value of each voxel minus the mean of the whole-brain CBF by the standard deviation (SD) of the whole-brain CBF ([voxel CBF–whole brain mean CBF]/[whole-brain CBF SD]).

Physiological Data Acquisition

During each of the 3 PCASL runs, heart rate, acquired with finger pulse oxymeter, and respiration, acquired with bellows, were collected with the physiological monitoring system integrated in the MR system. Analyzable heart rate data were acquired on 13 of the 14 subjects; all 14 subjects had useable respiration data. Heart rate and respiration were expressed as median beats or breaths per minute.

Rest and Cognitive Task Conditions

The PCASL protocol was acquired 3 times, each taking 6 min 49 s, and was run in the same order for all subjects: first rest (Rest 1), cognitive task (Task), and second rest (Rest 2). For both rest conditions, subjects were instructed to lie still, relaxed, and with eyes open. For the cognitive task condition, subjects performed blocks of a spatial working memory task, which involved visual presentation of memoranda (sequence of 3 or 6 spatially distributed positions), imposition of an 8-s retention interval of rest or an arithmetic or spatial tracking task, a 4.5-s recall interval for the 3-item sequences, and a 9-s recall interval for the 6-item sequences (Chanraud et al. 2010). Subjects used their right hand to respond by button box in the scanner; accuracy (percent correct accounting for accuracy and order of recall) and response time (in ms) were recorded for each trial.

Table 1
ROI used in this study and their anatomical sources

	Left			Right		
ASL_ROI	Tzourio-Mazoyer name	SRI24 code	Tzourio-Mazoyer code	Tzourio-Mazoyer name	SRI24 code	Tzourio-Mazoyer code
Lateral frontal	Precentral_L	1	2001	Precentral_R	2	2002
Lateral frontal	Frontal_Sup_L	3	2101	Frontal_Sup_R	4	2102
Lateral frontal	Frontal_Sup_Orb_L	5	2111	Frontal_Sup_Orb_R	6	2112
Lateral frontal	Frontal_Mid_L	7	2201	Frontal_Mid_R	8	2202
Lateral frontal	Frontal_Mid_Orb_L	9	2211	Frontal_Mid_Orb_R	10	2212
Lateral frontal	Frontal_Inf_Oper_L	11	2301	Frontal_Inf_Oper_R	12	2302
Lateral frontal	Frontal_Inf_Tri_L	13	2311	Frontal_Inf_Tri_R	14	2312
Lateral frontal	Frontal_Inf_Orb_L	15	2321	Frontal_Inf_Orb_R	16	2322
Lateral frontal	Rolandic_Oper_L	17	2331	Rolandic_Oper_R	18	2332
Lateral frontal	Supp_Motor_Area_L	19	2401	Supp_Motor_Area_R	20	2402
Medial frontal	Olfactory_L	21	2501	Olfactory_R	22	2502
Medial frontal	Frontal_Sup_Medial_L	23	2601	Frontal_Sup_Medial_R	24	2602
Medial frontal	Frontal_Med_Orb_L	25	2611	Frontal_Med_Orb_R	26	2612
Medial frontal	Rectus_L	27	2701	Rectus_R	28	2702
Insula	Insula_L	29	3001	Insula_R	30	3002
Cingulum_Ant + Mid	Cingulum_Ant_L	31	4001	Cingulum_Ant_R	32	4002
Cingulum_Ant + Mid	Cingulum_Mid_L	33	4011	Cingulum_Mid_R	34	4012
Cingulum_Post	Cingulum_Post_L	35	4021	Cingulum_Post_R	36	4022
Hippocampus + amygdala	Hippocampus_L	37	4101	Hippocampus_R	38	4102
Hippocampus + Amygdala	ParaHippocampal_L	39	4111	ParaHippocampal_R	40	4112
Hippocampus + Amygdala	Amygdala_L	41	4201	Amygdala_R	42	4202
Calcarine	Calcarine_L	43	5001	Calcarine_R	44	5002
Occipital	Cuneus_L	45	5011	Cuneus_R	46	5012
Occipital	Lingual_L	47	5021	Lingual_R	48	5022
Occipital	Occipital_Sup_L	49	5101	Occipital_Sup_R	50	5102
Occipital	Occipital_Mid_L	51	5201	Occipital_Mid_R	52	5202
Occipital	Occipital_Inf_L	53	5301	Occipital_Inf_R	54	5302
Parietal	Fusiform_L	55	5401	Fusiform_R	56	5402
Parietal	Postcentral_L	57	6001	Postcentral_R	58	6002
Parietal	Parietal_Sup_L	59	6101	Parietal_Sup_R	60	6102
Parietal	Parietal_Inf_L	61	6201	Parietal_Inf_R	62	6202
Parietal	SupraMarginal_L	63	6211	SupraMarginal_R	64	6212
Parietal	Angular_L	65	6221	Angular_R	66	6222
Parietal	Paracentral_Lobule_L	69	6401	Paracentral_Lobule_R	70	6402
Precuneus	Precuneus_L	67	6301	Precuneus_R	68	6302
Caudate+Putamen	Caudate_L	71	7001	Caudate_R	72	7002
Caudate+Putamen	Putamen_L	73	7011	Putamen_R	74	7012
Globus Pallidus	Pallidum_L	75	7021	Pallidum_R	76	7022
Thalamus	Thalamus_L	77	7101	Thalamus_R	78	7102
Temporal	Heschl_L	79	8101	Heschl_R	80	8102
Temporal	Temporal_Sup_L	81	8111	Temporal_Sup_R	82	8112
Temporal	Temporal_Pole_Sup_L	83	8121	Temporal_Pole_Sup_R	84	8122
Temporal	Temporal_Mid_L	85	8201	Temporal_Mid_R	86	8202
Temporal	Temporal_Pole_Mid_L	87	8211	Temporal_Pole_Mid_R	88	8212
Temporal	Temporal_Inf_L	89	8301	Temporal_Inf_R	90	8302
Cerebellum_Superior	Cerebellum_Crus1_L	91	9001	Cerebellum_Crus1_R	92	9002
Cerebellum_Superior	Cerebellum_3_L	95	9021	Cerebellum_3_R	96	9022
Cerebellum_Superior	Cerebellum_4_5_L	97	9031	Cerebellum_4_5_R	98	9032
Cerebellum_Superior	Cerebellum_6_L	99	9041	Cerebellum_6_R	100	9042
Cerebellum_Inferior	Cerebelum_Crus2_L	93	9011	Cerebellum_Crus2_R	94	9012
Cerebellum_Inferior	Cerebellum_7b_L	101	9051	Cerebellum_7b_R	102	9052
Cerebellum_Inferior	Cerebellum_8_L	103	9061	Cerebellum_8_R	104	9062
Cerebellum_Inferior	Cblm_Tonsil_9_L	105	9071	Cblm_Tonsil_9_R	106	9072
Cerebellum_Inferior	Cerebelum_10_L	107	9081	Cerebelum_10_R	108	9082
Vermis	Vermis_1	128	9100			
Vermis	Vermis_2	129	9110			
Vermis	Vermis_3	130	9120			

Note: Table is from Pfefferbaum et al. 2010.

Rest-to-Task-to-Rest CBF Regional Temporal Connectivity Analysis

A connectivity analysis using the 3 conditions, Rest 1–Task–Rest 2, in lieu of a traditional functional time series was conducted with the "conn" toolbox, implemented in SPM (http://www.fil.ion.ucl.ac.uk/spm/ext/). Normalized regional CBF images corresponding to the conditions Rest 1, Task, and Rest 2 were preprocessed using Statistical Parametric Mapping 8 (SPM8) software (Wellcome Department of Imaging Neuroscience). For each subject, skull-stripped images of normalized CBF and coregistered late-echo FSE were spatially normalized and resliced to 3 mm isotropic resolution, using normalization parameters issued from the normalization of gray matter segmented from the FSE images onto the gray matter template from the Montreal Neurological Institute. All image sequences were routinely inspected for normalization artifacts and finally, spatially smoothed with an 8-mm full-width at half-maximum Gaussian filter.

Seeded voxel correlations between the signal from a given seed and that at every brain voxel provided seed-to-voxel connectivity estimations using the CBF from the 3 conditions (Rest 1, Task, and Rest 2) as the temporal variable. The a priori selected seed was the left posterior cingulate region from the Tzourio-Mazoyer template (Tzourio-Mazoyer et al. 2002). Temporal connectivity maps were generated for each subject by estimating the correlation coefficient between all brain voxels and the seed signal across the conditions in a 2-sided analysis, showing both positive and negative correlation. These images were included in a second-level conjunctive group (between subjects), random-effects analysis. The magnitude and extent of temporal connectivity within the group were thresholded using a false discovery

rate correction of $P_{FDR} < 0.05$ for the whole brain volume with a minimum cluster extent of 30 contiguous voxels.

Statistical Analysis

Analyses used either raw (nonnormalized) or normalized CBF data. A series of 3-way within-subject analysis of variance (ANOVA), based on normalized CBF data, tested for differences between conditions and across ROIs in the left and right hemispheres. Each paired comparison was tested separately: Rest 1 versus Task, Rest 2 versus Task, and Rest 1 versus Rest 2. Where appropriate, Greenhouse-Geisser correction was used. Applying family-wise Bonferroni adjustment for 20 comparison (based on 19 bilateral and 1 midline ROIs) with alpha = 0.05 (2-tailed), the *P* value accepted as significant was 0.0025. Relations between regional CBF and performance and heart rate were examined with Pearson correlations; the family-wise Bonferroni adjustment with alpha = 0.05 (2-tailed) was applied to determine statistical significance.

Results

Global CBF

Global CBF was the nonnormalized sum of all voxels in the computed flow images within the skull-stripped brain mask, which included all cortical, subcortical, and cerebellar tissue and CSF (Fig. 1). A repeated-measures ANOVA, comparing global CBF in mL/100cc/min, across the 3 conditions revealed a significant condition effect ($F_{2,26} = 4.198$, $P = 0.0263$). Follow-up comparisons showed a small but significant increase from Rest 1 (mean ± standard error [SE] = 37.15 ± 1.55) to Task (mean ± SE = 38.12 ± 1.69) conditions, followed by a decrease back to baseline levels at Rest 2 (mean ± SE = 36.92 ± 1.46).

Average Total and Regional Nonnormalized Cortical CBF in Each Condition

The average, nonnormalized, total cortical CBF was marginally different across the 3 runs ($F_{2,41} = 3.331$, $P = 0.0516$). Expressed as mL/100cc of gray matter/min, the mean ± SE for the first rest condition (Rest 1) was 46.76 ± 2.04, the Task condition was 47.88 ± 2.26, and the second rest condition (Rest 2) was 46.47 ± 1.96. Across the 3 conditions, the intraclass correlation (ICC), an index of repeatability, was 0.956. The difference between the Task and Rest 2 conditions ($F_{1,27} = 4.85$, $P = 0.0463$) was marginally larger than that between the Task and Rest 1 conditions ($F_{1,27} = 3.965$, $P = 0.068$). The difference between the 2 rest conditions, however, was not significant ($F_{1,27} = 0.313$, $P = 0.59$) and their ICC = 0.968.

Regional CBF ranged from ~25 to 60 mL/100cc of gray matter or tissue/min across the brain. Despite increases in some and decreases in other brain regions from rest to task, the relative ranking of CBF remained essentially the same across brain regions (Fig. 2).

Differences between Task Conditions in Normalized Regional CBF

The first within-subject condition-by-region-by-laterality ANOVA examined differences between the Rest 1 and Task conditions. All 3 effects and each pair of interactions were significant ($P = 0.004$ to 0.0001) as was the 3-way interaction ($F_{15,195} = 90.892$, $P = 0.0001$). Taken together with follow-up *t*-tests of the mean regional normalized CBF differences between conditions (Fig. 3), these effects and interactions indicate significantly "decreased" activation from rest to task in the medial frontal, temporal, anterior and posterior cingulate, and precuneus ROIs, significant bilaterally for all except the right temporal ROI. At the same time, activation was "increased" in the occipital, calcarine, and superior and inferior cerebellar ROIs, significant for all on the right and bilaterally in the calcarine ROI. Of the 16 primary bilateral ROIs examined, mean deactivation of 7 ROIs and mean activation of 5 other ROIs were greater in the left than the right hemisphere, giving rise to significant laterality effects and interaction in the ANOVA (Fig. 3).

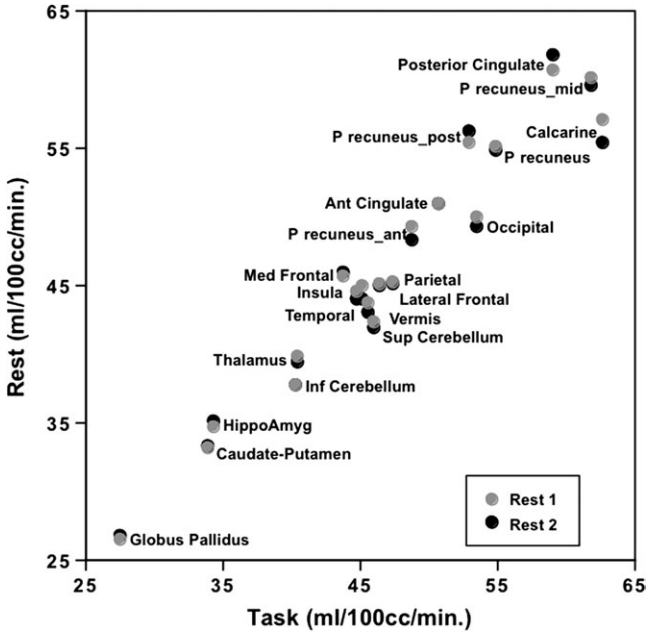

Figure 2. Correlations between the average nonnormalized regional CBF across the 14 subjects in each rest conditions and the task condition. The highest CBF values were in the posterior cingulate, precuneus, and calcarine cortices during rest and task, although these values were relatively diminished during the task. Note that the values for the anterior cingulum and inferior cerebellum at Rest 1 and Rest 2 are overlapping.

The second 3-way ANOVA examined differences between the Rest 2 and Task conditions and yielded a similar pattern of significant effects, interactions, and follow-up regional differences as based on the Rest 1–Task comparison. Again, all 3 effects and each pair of interactions were significant ($P = 0.009$ to 0.0001) as was the 3-way interaction ($F_{15,195} = 3.557$, $P = 0.0118$). The few differences in activation–deactivation patterns between Task–Rest 1 and Task–Rest 2 conditions were identified with follow-up tests by ROI. These paired *t*-tests (family-wise Bonferroni-corrected $P \leq 0.0025$) for the Task–Rest 2 comparisons revealed that the right hippocampal–amygdala ROI showed deactivation in the right hemisphere and that the left rather than the right occipital and superior cerebellar ROI showed activation. Of the 16 bilateral ROIs, mean deactivation of 4 ROIs and mean activation of 4 other ROIs were greater in the left than the right hemisphere, again giving rise to significant laterality effects and interaction in the ANOVA (Fig. 3).

The third 3-way ANOVA examined differences between the first and second rest conditions. Neither the condition effect ($P = 0.476$) nor the 3-way interaction was significant ($F_{15,195} = 0.439$, $P = 0.416$).

Parcellated Precuneus

Given the heterogeneity of perfusion levels within the precuneus and recently described differentiation of projection distributions from this anatomically heterogeneous structure (Margulies et al. 2009), we measured perfusion in 3 subparcellated regions of each hemisphere: anterior, middle, and

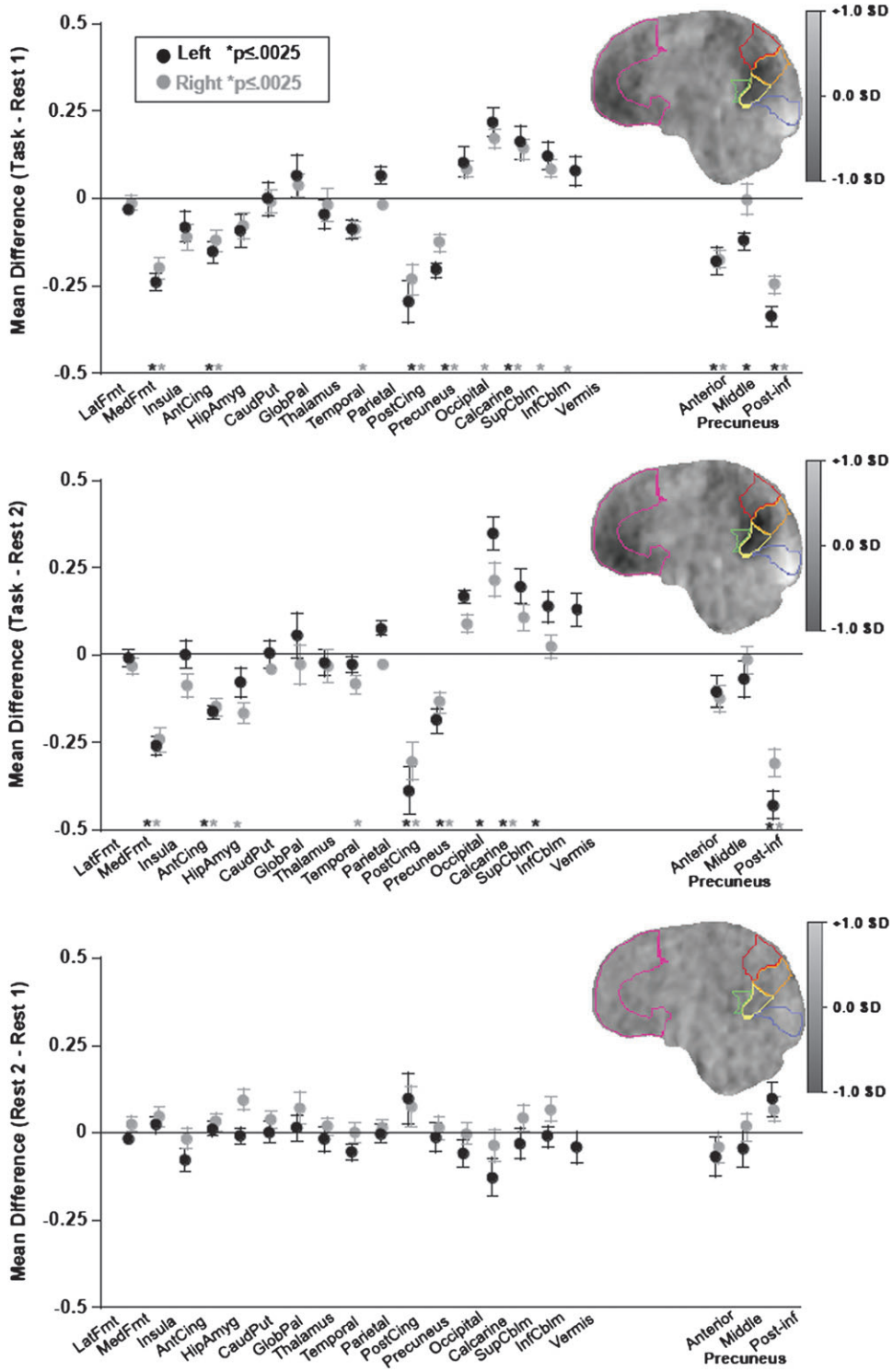

Figure 3. Mean ± SE standardized differences in CBF for each lateralized and midline ROI and parcellated precuneus for each task pairs: Top: Task − Rest 1; middle: Task − Rest 2; and bottom: Rest 2 − Rest 1. The sagittal images are CBF differences averaged across the 14 subjects. Magenta, medial frontal cortex; red, anterior precuneus; orange, middle precuneus; yellow, posterior–inferior precuneus; green, posterior cingulate; blue, calcarine cortex.

posterior inferior (Fig. 3). A series of 3-way ANOVAs examined regional differences between each pair of conditions. The Rest 1 versus Task ANOVA and the Rest 2 versus Task ANOVA yielded the same pattern of results, with significant simple effects of task condition, ROI, and laterality ($P = 0.0001$ for all effects) and 3-way interactions (Rest 1 vs. Task $F_{2,26} = 4.090$, $P = 0.0286$; Rest 2 vs. Task $F_{2,26} = 4.792$, $P = 0.0169$). In both comparisons, engagement in the task "deactivated" all 3 regions of this ROI but had consistent significant and largest effects in the posterior–inferior precuneus, with left greater than right.

The Rest 1 versus Rest 2 ANOVA failed to identify a significant 3-way interaction ($F_{2,26} = 1.389$, $P = 0.2672$). A significant

condition-by-ROI ($F_{2,26} = 6.327$, $P = 0.0175$) interaction indicated a small but statistically significant difference between Rest 1 and Rest 2, with some lower and some higher. Nonetheless, none of the follow-up paired comparisons for any ROI survived family-wise Bonferroni correction of alpha.

Nodes of the Default Mode Network: Normalized and Absolute CBF

Three major ROIs of the default network—posterior cingulate cortex, posterior–inferior precuneus, and medial frontal cortices—were consistently affected by the rest-to-task-to-rest manipulation across all subjects (Fig. 4). Of the 168 values (3 structures, 2 hemispheres, 2 rest–task comparisons, and 14 subjects), 165 were higher in the rest than task conditions (binomial test $Z = 12.499$, $P < 10^{-5}$).

Separate ANOVAs of nonnormalized CBF for each of the 3 major ROIs (posterior cingulate, posterior–inferior precuneus, and medial frontal) for each hemisphere confirmed that the pattern observed with normalized CBF was a reflection of absolute changes in CBF (Fig. 5). The task–rest effect was significant for 5 of the 6 comparisons (3 meet Bonferroni criterion for multiple comparisons): posterior cingulate left $P = 0.0422$, right $P = 0.0995$; posterior–inferior precuneus left $P = 0.0001$, right $P = 0.0029$; medial frontal left $P = 0.0005$, right $P = 0.0271$.

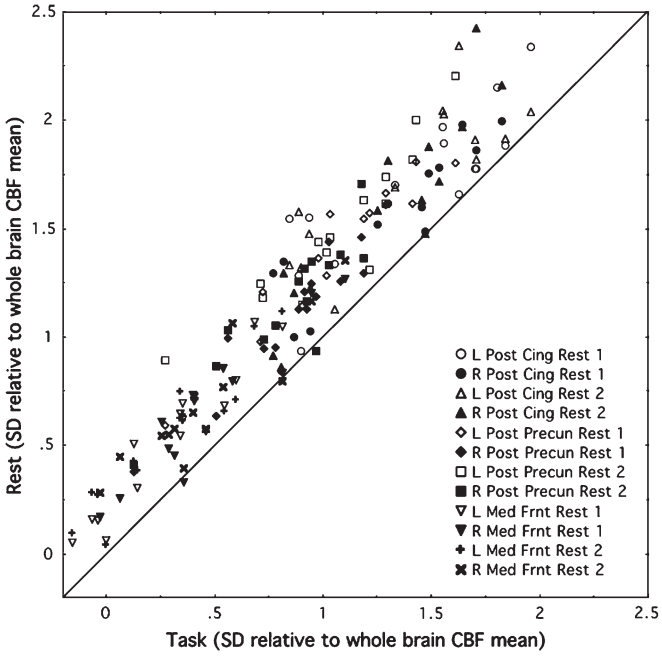

Figure 4. Relation between normalized CBF values in the rest and task conditions for the posterior cingulate cortex, posterior–inferior precuneus, and medial frontal cortices in each hemisphere. Of the 168 values of the 14 subjects, 165 were higher in the rest conditions than task condition.

Rest–Task–Rest CBF Regional Temporal Connectivity Analysis

Overall, the conjunctive group analysis revealed a robust and significant pattern of temporal connectivity (i.e., rest-to-task-to-rest) with the left posterior cingulate region reproducing the spatial topography of the 2 networks described in the previous analysis (Fig. 6). Rest–task–rest temporal CBF fluctuations of the left posterior cingulate region were positively correlated principally with regions in the default mode network, including the right middle orbital and superior medial frontal gyri, bilateral anterior and median cingulate cortex, right posterior cingulate gyrus, bilateral precuneus, bilateral Heschl's gyrus, right rolandic operculum, bilateral superior, and middle temporal gyri (Table 2). Conversely, the left posterior cingulate CBF was negatively correlated with CBF in posterior regions, including bilateral lingual, superior occipital, and calcarine cortices, left superior and inferior parietal gyri, left inferior occipital gyrus, right middle temporal gyrus, and cerebellar crus I (Table 2).

Cognitive Performance and Correlates of Task Performance

Cognitive test accuracy scores and response times showed the expected pattern, providing assurance that the subjects were

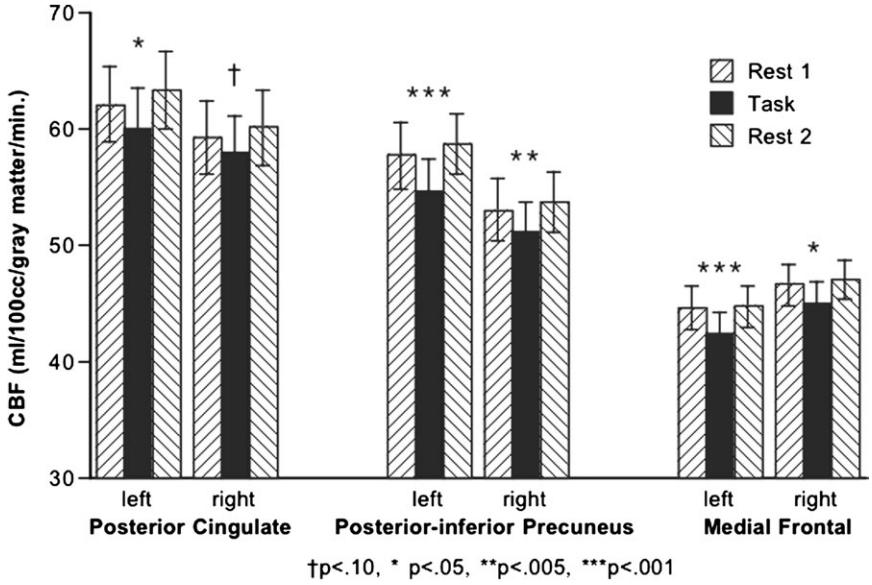

Figure 5. Mean ± SE absolute CBF for each lateralized ROI of 3 principal nodes of the default mode network at the 3 measurements: Rest 1, Task, and Rest 2. Significance values are from repeated-measures ANOVAs.

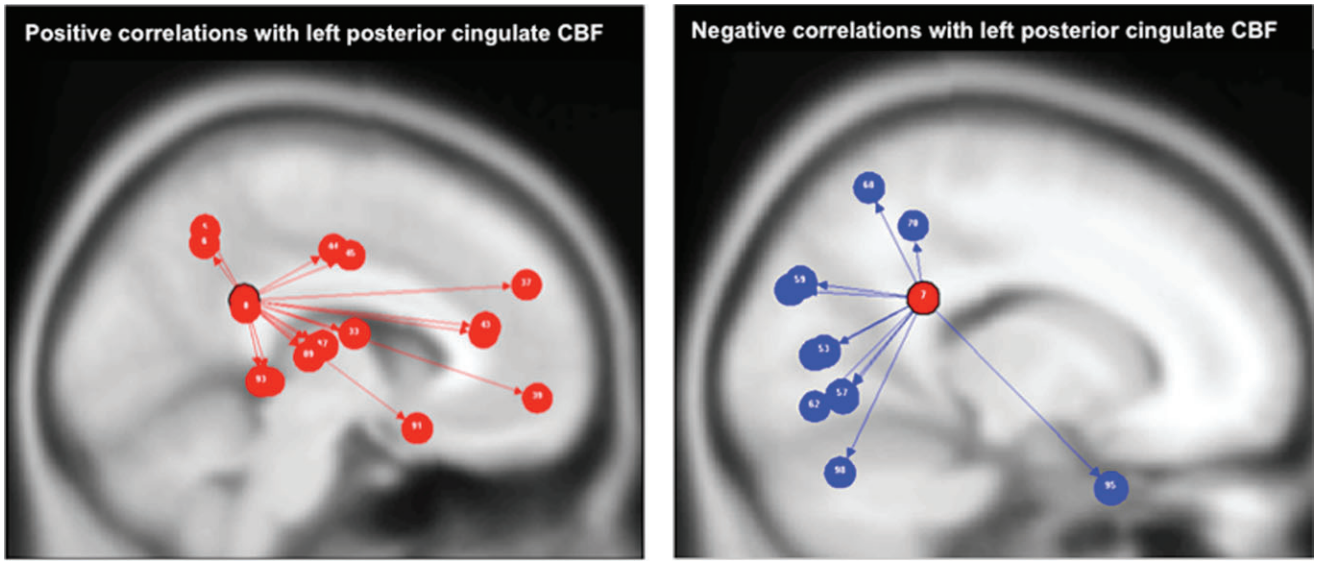

Figure 6. Rest–Task–Rest temporal connectivity. Top: regions with temporal fluctuations (Rest–Task–Rest) that correlated positively ($P < 0.05$ FDR) with left posterior cingulate CBF, that is, regions of task-dependent CBF deactivation. Bottom: regions with temporal fluctuations (Rest–Task–Rest) that correlated negatively with left posterior cingulate CBF, that is, regions of task-dependent CBF activation. Table 2 presents the connectivity statistics.

Table 2
Rest–task–rest temporal connectivity correlations with the left posterior cingulate cortex

Brain regions	Cluster level β	*t*-value	*P* FDR
Positive correlations			
Right middle orbital frontal gyrus	18.37	$>10^4$	<0.0001
Left anterior cingulate gyrus	18.37	$>10^4$	<0.0001
Right Heschl's gyrus	18.37	$>10^4$	<0.0001
Right median cingulate gyrus	18.35	$>10^4$	<0.0001
Right rolandic operculum	15.74	6.00	<0.001
Right superior medial frontal gyrus	15.74	6.00	<0.001
Right anterior cingulate gyrus	15.74	6.00	<0.001
Right superior temporal gyrus	15.74	6.00	<0.001
Left precuneus	15.73	6.00	<0.001
Left median cingulate gyrus	15.73	6.00	<0.001
Right precuneus	13.17	3.74	0.01
Right posterior cingulate gyrus	13.12	3.68	0.01
Left superior temporal gyrus	13.12	3.68	0.01
Right middle temporal gyrus	13.12	3.68	0.01
Left Heschl gyrus	13.09	3.67	0.01
Left middle temporal gyrus	13.04	3.67	0.01
Negative correlations			
Right lingual gyrus	−18.37	$>10^4$	<0.0001
Left inferior parietal gyrus	−18.37	$>10^4$	<0.0001
Left superior parietal gyrus	−15.77	−6.07	<0.001
Left calcarine cortex	−15.74	−6.00	<0.001
Left lingual gyrus	−15.74	−6.00	<0.001
Left inferior occipital gyrus	−15.74	−6.00	<0.001
Right middle temporal gyrus	−15.74	−6.00	<0.001
Cerebellum crus I	−15.73	−6.00	<0.001
Right calcarine cortex	−15.69	−5.99	<0.001
Right superior occipital gyrus	−13.13	−3.69	0.015
Left superior occipital gyrus	−13.12	−3.68	0.015

performing the task. Specifically, scores were higher and response times faster with the memory load of 3 than 6 and without a retention interval distraction task than with one (Fig. 7). Ceiling effects and skewed distributions of accuracy scores precluded investigation of correlations between accuracy and regional CBF.

Exploratory correlational analyses were conducted, however, on response times in the 6-item conditions involving arithmetic and tracking distractor tasks and CBF during the Task condition. Faster response times in the working memory task with tracking distraction showed a number of correlations with regional CBF, the most robust being between faster response times and higher CBF in the left globus pallidus ($r = -0.68$, $P = 0.008$), in keeping with the fact that all subjects were right handed and used their right hand to perform the task. Faster response times in the working memory task with arithmetic distraction correlated with higher right temporal CBF ($r = -0.67$, $P = 0.0085$), in keeping with the spatial nature of the task (Fig. 7). Multiple regression analysis examined the independent contributions the right temporal and left globus pallidus CBF made to response times in the 2 spatial working memory distraction conditions. CBF in these brain regions together accounted for 64% of the response time variance ($P = 0.0037$) in the spatial working memory task with arithmetic distraction, with a greater independent contribution from the temporal ($t = 3.301$, $P = 0.0071$) than the globus pallidus ($t = 2.382$, $P = 0.0364$) CBF. Conversely, CBF in these 2 brain regions accounted for 67% of the response time variance ($P = 0.0023$) in the memory task with tracking distraction, with a greater independent contribution from the globus pallidus ($t = 3.445$, $P = 0.0055$) than the temporal ($t = 2.657$, $P = 0.0223$) CBF.

Additional but weaker correlations emerged between faster response times in the tracking distraction condition and higher CBF in the temporal (right $r = -0.56$, $P = 0.0381$), anterior cingulate (right $r = -0.54$, $P = 0.0461$), insular (right $r = -0.62$, $P = 0.0188$), globus pallidus (right $r = -0.58$, $P = 0.0316$), and caudate–putamen (right $r = -0.58$, $P = 0.0306$) ROIs and with lower CBF in the occipital ROI (right $r = 0.58$, $P = 0.0314$). Performance scores did not correlate significantly with any regional CBF at Rest 1 or Rest 2.

Physiological Measurements and Correlates of Regional CBF

A repeated-measures ANOVA revealed that heart rate, expressed as median beats per minute, increased significantly with task compared with both rest conditions ($F_{2,38} = 8.358$, $P = 0.0018$). Follow-up tests showed that heart rate in the 2 rest conditions did not statistically differ (Fig. 8). Median

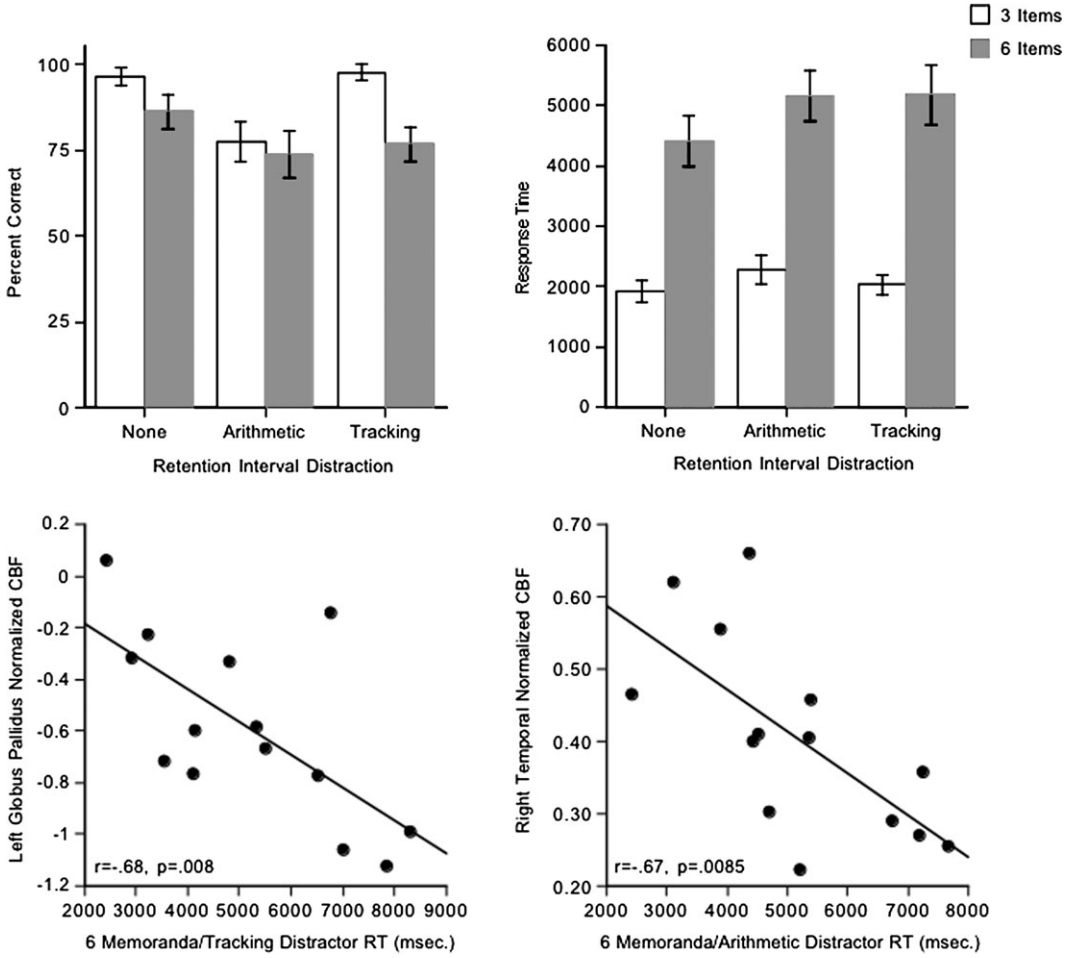

Figure 7. Top: mean ± SE of percent correct (left) and response times (right) for the 3- and 6-memoranda spatial working memory test in each of the 3 retention interval conditions. Bottom: correlations between (left) the left globus pallidus CBF and the 6-memoranda task with the tracking distractor and (right) the right temporal CBF and the 6-memoranda task with the arithmetic distractor.

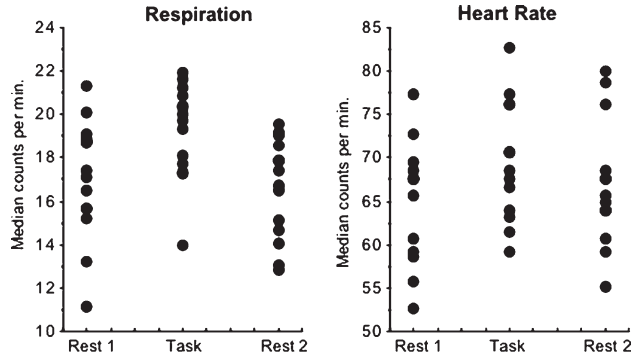

Figure 8. Respiration and heart rate, expressed as median counts per minute for each subject during each PCASL run. Note that heart rate values were valid for 13 of the 14 subjects.

respiration values showed the same pattern of change in task versus rest conditions ($F_{2,41}$ = 11.089, P = 0.0003). Heart rate and respiration did not correlate significantly with each other in any imaging condition. Despite these physiological changes with task demands, neither heart rate nor respiration correlated significantly with global CBF or any normalized or raw (nonnormalized) measure of CBF in any ROI for any task or rest condition.

Discussion

Whole-brain blood flow measurement with PCASL and a simple block design of ~7-min acquisition of rest–task–rest revealed a strong pattern of CBF decrease (deactivation) in the classic default mode network and CBF increase (activation) posteriorly, primarily in visual cortex and superior cerebellum. This activation–deactivation pattern was demonstrated with a priori ROI analysis and a novel application of an SPM correlational connectivity analysis. Examination of laterality effects suggested a more dynamic role for left than right hemisphere in the patterns of activation–deactivation. Along with deactivation in the posterior cingulate region, parcellation of the precuneus into anterior, middle, and posterior–inferior regions revealed deactivation in the posterior–inferior but not middle or anterior precuneus and equally large as the posterior cingulate cortex.

Use of normalized values put regional blood flow values for all ROIs on the same scale, thereby enabling direct comparisons to be made across individuals and ROIs, even those with substantially different baseline perfusion levels, and across imaging conditions, for which absolute global CBF showed a small but statistically significant increase from rest to task. The normalized values take into account the absolute increase in global CBF during task compared with rest. Furthermore,

unlike measures requiring contrasts for deriving activation quantification, normalized PCASL values were calculated for each imaging condition, thus permitting quantification of regional CBF per condition rather than as differences.

Global CBF varies considerably across individuals and within the same individuals across days, probably caused by a number of factors, such as variation in cardiovascular status, pulse, respiration, level of anxiety, and caffeine and nicotine consumption (for review, D'Esposito et al. 2003). Nonetheless, the relative distribution of CBF in various parts of the brain is consistent from day-to-day in the resting state (e.g., Aguirre et al. 2002; Wang et al. 2003; Parkes et al. 2004; MacIntosh et al. 2008; Petersen et al. 2010; Pfefferbaum et al. 2010; Xu et al. 2010). In the current study, an omnibus test of Rest 2 compared with Rest 1 across the whole brain showed considerable repeatability. Furthermore, the normalized regional decreases in CBF from Rest 1 to Task and increase from Task to Rest 2 were highly consistent across individuals, occurring in 165 of 168 observations in 3 nodes of the default network (left and right posterior cingulate, posterior–inferior precuneus, and medial frontal cortex). Activity in the precuneus/posterior cingulate node of a connectivity analysis were identified as the only one in the default network that correlated with nearly all other nodes whether at rest or while engaged in an activity (Fransson and Marrelec 2008). Other studies using fMRI and spontaneous or evoked BOLD response to examine intrinsic connectivity in rest and active task states comport with the results reported herein indicating activity in selective nodes of a functional network correlated in both rest and activity conditions, thereby suggesting stability of identified networks (e.g., Buckner et al. 2009).

Previous ASL studies have used T_2-weighted echo-planar imaging (EPI), 2D multislice strategies to explore the resting state. Chuang et al. (2008) proposed a method to control the substantial T_2^*-weighting (BOLD) contribution to EPI-acquired continuous ASL data and demonstrated high correlation between BOLD and ASL in sensorimotor cortex at rest and during a sequential finger opposition task. Lim et al. (2009) used a task–rest–task design with a visual vigilance and attention task with low-cognitive demands. From the first rest to task, CBF decreased not only in precuneus/posterior cortex, that is, nodes of the default mode network but also bilateral occipital cortex, not normally considered part of the default mode network but observed in an FDG PET activation study of the vestibular-ocular response (Wenzel et al. 1996) and the seminal explication of the default mode network (Raichle et al. 2001). Task-related CBF decreases in nodes of the default mode network, however, do not necessarily indicate lower activity in those regions than occurs during task-related activity in other brain regions. Rather, the decreases could be transient from a baseline level rather than a return to baseline after an unexpected activation (Raichle et al. 2001). The post-task rest condition of Lim et al. (2009) compared with the pretask rest showed robust deactivation in several nodes of the default mode network; these data did not show a robust return to the default mode network pattern of CBF as seen in our data and were interpreted as a fatigue effect. Our task, while not so long (~7 vs. 20 min) but more cognitively challenging, did not produce this "fatigue pattern." Zou et al. (2009) demonstrated dynamic and static functional connectivity consistent with the default mode network in the resting state but did not compare the resting state with a task to ascertain whether a cognitive challenge would reveal an absolute decrease in CBF in nodes of the default mode network. In contrast to these T_2^*-dependent studies, we employed a T_1-dependent 3D spiral ASL acquisition with full brain coverage and a requisite cognitive challenge to the default mode network (cf. Greicius et al. 2003) and demonstrated a post-task return to the default mode network pattern of CBF. Our interleaved 3D spiral PCASL acquisition takes several minutes and is not conducive to a time series analysis based on TRs of a few seconds, but unlike T_2-weighted EPI with 2D multislice strategies, it does not present the problem of echo-planar spatial distortion or T_2^*-weighted BOLD contamination.

The effect size of deactivation of the default network from rest to task assessed with PCASL ranged from 0.3 to nearly 0.5 SD in the posterior cingulate and posterior–inferior precuneus regions. The deactivation pattern observed with PCASL was similar to that reported with resting state BOLD, but the change in CBF was on the order of 10%, which is in contrast to smaller effects typically observed with BOLD. Others have reported even larger dynamic CBF responses, which were elicited with a cognitive task (Mildner et al. 2005). Bold can produce 1–3% signal changes, whereas the ASL CBF signal is less than 1% of the equilibrium MRI intensity, and a 10% change of that is equivalent to a 0.1% change of the equilibrium MRI intensity. With regard to thermal noise, BOLD has the advantage. If noise is from motion or subject instability, the larger fractional ASL signal change is an advantage. For stimulations longer than 3 min, and even shorter durations in less cooperative subjects, the instability in BOLD tends to make ASL preferable (Aguirre et al. 2002). Thus the PCASL acquisition approach may be particularly useful in studies of children and neuropsychiatric patients, who as a group often present signal-to-noise ratio challenges in activation studies.

The posterior cingulate cortex is highly heterogeneous both anatomically and functionally and is a central component of the default mode network (Vogt et al. 2006). Similarly, the recently described differentiation of projection distributions of the posterior portion of the anatomically heterogeneous precuneus are sites of high intrinsic task-free functional brain activity demonstrated with BOLD (Margulies et al. 2009) in nodes of the default mode network. The large task-related CBF decrease in the posterior–inferior precuneus relative to its anterior and middle portions adds further evidence for the heterogeneity of this cortical region. In the current study, the regions with the largest task-induced deactivation (left and right posterior cingulate and posterior–inferior precuneus) were also among the regions with the highest CBF at rest (Pfefferbaum et al. 2010); the greatest difference in absolute CBF from intrinsic to evoked activity was a 7% decline in the left precuneus that was followed by a 6.2% return to resting state. Despite this large task-related CBF difference, even during the task CBF was higher in the posterior nodes of the default mode network than the cortical average across the whole brain. This suggests that when an individual is in the default mode, these regions are indeed activated as indexed by high relative and absolute CBF, which is in turn reduced but still at high levels during task performance and with some higher than most other cortical regions. We speculate that the difference in regional CBF between the intrinsic (resting) and evoked (task) activity levels could represent functional readiness or reserve that is vulnerable to diminution by conditions affecting perfusion,

including normal aging, hypertension, dementia, and alcohol and drug dependence.

Funding

National Institutes of Health (AA012388, AA005965, AA010723, AA017923, AG017919, EB008381, MH80729).

Notes

Conflict of Interest: Drs Pfefferbaum, Chanraud, Pitel, Müller-Oehring, and Sullivan have no conflicts of interest with this work, either financial or otherwise. Dr Shankaranarayanan is an employee of General Electric Healthcare, the manufacturer of the MR system used in this study. Dr Alsop is an inventor on patents related to the ASL protocols used herein and may receive patent-related royalties.

References

Aguirre GK, Detre JA, Zarahn E, Alsop DC. 2002. Experimental design and the relative sensitivity of BOLD and perfusion fMRI. Neuroimage. 15:488–500.

Alsop DC, Detre JA, D'Esposito M, Howard RS, Maldjian JA, Grossman M, Listerud J, Flamm ES, Judy KD, Atlas SW. 1996. Functional activation during an auditory comprehension task in patients with temporal lobe lesions. Neuroimage. 4:55–59.

Andrews-Hanna JR, Reidler JS, Sepulcre J, Poulin R, Buckner RL. 2010. Functional-anatomic fractionation of the brain's default network. Neuron. 65:550–562.

Bangen KJ, Restom K, Liu TT, Jak AJ, Wierenga CE, Salmon DP, Bondi MW. 2009. Differential age effects on cerebral blood flow and BOLD response to encoding: associations with cognition and stroke risk. Neurobiol Aging. 30:1276–1287.

Buckner RL, Andrews-Hanna JR, Schacter DL. 2008. The brain's default network: anatomy, function, and relevance to disease. Ann N Y Acad Sci. 1124:1–38.

Buckner RL, Sepulcre J, Talukdar T, Krienen FM, Liu H, Hedden T, Andrews-Hanna JR, Sperling RA, Johnson KA. 2009. Cortical hubs revealed by intrinsic functional connectivity: mapping, assessment of stability, and relation to Alzheimer's disease. J Neurosci. 29:1860–1873.

Buxton RB, Wong EC, Frank LR. 1998. Dynamics of blood flow and oxygenation changes during brain activation: the balloon model. Magn Reson Med. 39:855–864.

Chanraud S, Pitel AL, Rohlfing T, Pfefferbaum A, Sullivan EV. 2010. Dual tasking and working memory in alcoholism: Relation to frontocerebellar circuitry. Neuropsychopharmacology. Epub ahead of print April 21; doi: 101038/npp.2010.56.

Chuang KH, van Gelderen P, Merkle H, Bodurka J, Ikonomidou VN, Koretsky AP, Duyn JH, Talagala SL. 2008. Mapping resting-state functional connectivity using perfusion MRI. Neuroimage. 40:1595–1605.

Crovitz HF, Zener KA. 1962. Group test for assessing hand and eye dominance. Am J Psychol. 75:271–276.

D'Esposito M, Deouell LY, Gazzaley A. 2003. Alterations in the BOLD fMRI signal with ageing and disease: a challenge for neuroimaging. Nat Rev Neurosci. 4:863–872.

Dai W, Garcia D, de Bazelaire C, Alsop DC. 2008. Continuous flow-driven inversion for arterial spin labeling using pulsed radio frequency and gradient fields. Magn Reson Med. 60: 1488–1497.

Damoiseaux JS, Greicius MD. 2009. Greater than the sum of its parts: a review of studies combining structural connectivity and resting-state functional connectivity. Brain Struct Funct. 213:525–533.

Detre JA, Leigh JS, Williams DS, Koretsky AP. 1992. Perfusion imaging. Magn Reson Med. 23:37–45.

Detre JA, Wang J, Wang Z, Rao H. 2009. Arterial spin-labeled perfusion MRI in basic and clinical neuroscience. Curr Opin Neurol. 22:348–355.

Fox MD, Zhang D, Snyder AZ, Raichle ME. 2009. The global signal and observed anticorrelated resting state brain networks. J Neurophysiol. 101:3270–3283.

Fransson P. 2006. How default is the default mode of brain function? Further evidence from intrinsic BOLD signal fluctuations. Neuropsychologia. 44:2836–2845.

Fransson P, Marrelec G. 2008. The precuneus/posterior cingulate cortex plays a pivotal role in the default mode network: evidence from a partial correlation network analysis. Neuroimage. 42:1178–1184.

Garcia DM, Duhamel G, Alsop DC. 2005. Efficiency of inversion pulses for background suppressed arterial spin labeling. Magn Reson Med. 54:366–372.

Garraux G, Hallett M, Talagala SL. 2005. CASL fMRI of subcortico-cortical perfusion changes during memory-guided finger sequences. Neuroimage. 25:122–132.

Greicius MD, Krasnow B, Reiss AL, Menon V. 2003. Functional connectivity in the resting brain: a network analysis of the default mode hypothesis. Proc Natl Acad Sci U S A. 100:253–258.

Greicius MD, Srivastava G, Reiss AL, Menon V. 2004. Default-mode network activity distinguishes Alzheimer's disease from healthy aging: evidence from functional MRI. Proc Natl Acad Sci U S A. 101:4637–4642.

Greicius MD, Supekar K, Menon V, Dougherty RF. 2009. Resting-state functional connectivity reflects structural connectivity in the default mode network. Cereb Cortex. 19:72–78.

Herscovitch P, Raichle ME. 1985. What is the correct value for the brain–blood partition coefficient for water? J Cereb Blood Flow Metab. 5:65–69.

Jarnum H, Steffensen EG, Knutsson L, Frund ET, Simonsen CW, Lundbye-Christensen S, Shankaranarayanan A, Alsop DC, Jensen FT, Larsson EM. 2010. Perfusion MRI of brain tumours: a comparative study of pseudo-continuous arterial spin labelling and dynamic susceptibility contrast imaging. Neuroradiology. 52:307–317.

Kelly ME, Blau CW, Griffin KM, Gobbo OL, Jones JF, Kerskens CM. 2010. Quantitative functional magnetic resonance imaging of brain activity using bolus-tracking arterial spin labeling. J Cereb Blood Flow Metab. 30:913–922.

Kim M, Ducros M, Carlson T, Ronen I, He S, Ugurbil K, Kim DS. 2006. Anatomical correlates of the functional organization in the human occipitotemporal cortex. Magn Reson Imaging. 24:583–590.

Krienen FM, Buckner RL. 2009. Segregated fronto-cerebellar circuits revealed by intrinsic functional connectivity. Cereb Cortex. 19:2485–2497.

Leniger-Follert E, Hossmann KA. 1977. Microflow and cortical oxygen pressure during and after prolonged cerebral ischemia. Brain Res. 124:158–161.

Likar B, Viergever MA, Pernus F. 2001. Retrospective correction of MR intensity inhomogeneity by information minimization. EEE Trans Med Imaging. 20:1398–1410.

Lim J, Wu WC, Wang J, Detre JA, Dinges DF, Rao H. 2009. Imaging brain fatigue from sustained mental workload: an ASL perfusion study of the time-on-task effect. Neuroimage. 49:3426–3435.

MacIntosh BJ, Pattinson KT, Gallichan D, Ahmad I, Miller KL, Feinberg DA, Wise RG, Jezzard P. 2008. Measuring the effects of remifentanil on cerebral blood flow and arterial arrival time using 3D GRASE MRI with pulsed arterial spin labelling. J Cereb Blood Flow Metab. 28:1514–1522.

Margulies DS, Vincent JL, Kelly C, Lohmann G, Uddin LQ, Biswal BB, Villringer A, Castellanos FX, Milham MP, Petrides M. 2009. Precuneus shares intrinsic functional architecture in humans and monkeys. Proc Natl Acad Sci U S A. 106:20069–20074.

Mazoyer B, Zago L, Mellet E, Bricogne S, Etard O, Houde O, Crivello F, Joliot M, Petit L, Tzourio-Mazoyer N. 2001. Cortical networks for working memory and executive functions sustain the conscious resting state in man. Brain Res Bull. 54:287–298.

Mildner T, Zysset S, Trampel R, Driesel W, Moller HE. 2005. Towards quantification of blood-flow changes during cognitive task activation using perfusion-based fMRI. Neuroimage. 27:919–926.

Minoshima S, Giordani B, Berent S, Frey KA, Foster NL, Kuhl DE. 1997. Metabolic reduction in the posterior cingulate cortex in very early Alzheimer's disease. Ann Neurol. 42:85–94.

Parkes LM, Rashid W, Chard DT, Tofts PS. 2004. Normal cerebral perfusion measurements using arterial spin labeling: reproducibility, stability, and age and gender effects. Magn Reson Med. 51:736–743.
Petersen ET, Mouridsen K, Golay X. 2010. The QUASAR reproducibility study, Part II: results from a multi-center Arterial Spin Labeling test–retest study. Neuroimage. 49:104–113.
Pfefferbaum A, Chanraud S, Pitel A-L, Shankaranarayanan A, Alsop D, Rohlfing T, Sullivan EV. Forthcoming 2010. Volumetric cerebral perfusion imaging in healthy adults: regional distribution, laterality, and repeatability of pulsed continuous arterial spin labeling (PCASL). Psychiatry Res: Neuroimaging.
Popa D, Popescu AT, Pare D. 2009. Contrasting activity profile of two distributed cortical networks as a function of attentional demands. J Neurosci. 29:1191–1201.
Raichle ME. 2009. A paradigm shift in functional brain imaging. J Neurosci. 29:12729–12734.
Raichle ME, Gusnard DA. 2005. Intrinsic brain activity sets the stage for expression of motivated behavior. J Comp Neurol. 493:167–176.
Raichle ME, MacLeod AM, Snyder AZ, Powers WJ, Gusnard DA, Shulman GL. 2001. A default mode of brain function. Proc Natl Acad Sci U S A. 98:676–682.
Raichle ME, Snyder AZ. 2007. A default mode of brain function: a brief history of an evolving idea. Neuroimage. 37:1083–1090. discussion 1097–1099.
Rohlfing T, Maurer CR, Jr. 2005. Multi-classifier framework for atlas-based image segmentation. Pattern Recognit Lett. 26:2070–2079.
Rohlfing T, Maurer CR, Jr. Bluemke DA, Jacobs MA. 2003. Volume-preserving nonrigid registration of MR breast images using free-form deformation with an incompressibility constraint. IEEE Trans Med Imaging. 22:730–741.
Rohlfing T, Zahr NM, Sullivan EV, Pfefferbaum A. 2010. The SRI24 multi-channel atlas of normal adult human brain structure. Hum Brain Mapp. 31:798–819.
Rueckert D, Sonoda LI, Hayes C, Hill DL, Leach MO, Hawkes DJ. 1999. Nonrigid registration using free-form deformations: application to breast MR images. IEEE Trans Med Imaging. 18:712–721.
Smith S. 2002. Fast robust automated brain extraction. Hum Brain Mapp. 27:2349–2356.
Seeley WW, Menon V, Schatzberg AF, Keller J, Glover GH, Kenna H, Reiss AL, Greicius MD. 2002. Dissociable intrinsic connectivity networks for salience processing and executive control. J Neurosci. 17:143–155.
Shulman GL, Fiez JA, Corbetta M, Buckner RL, Miezin FM, Raichle ME, Petersen SE. 1997. Common blood flow changes across visual tasks: II. Decreases in cerebral cortex. J Cogn Neurosci. 9:648–663.
Talagala SL, Noll DC. 1998. Functional MRI using steady-state arterial water labeling. Magn Reson Med. 39:179–183.
Tzourio-Mazoyer N, Landeau B, Papathanassiou D, Crivello F, Etard O, Delcroix N, Mazoyer B, Joliot M. 2002. Automated anatomical labeling of activations in SPM using a macroscopic anatomical parcellation of the MNI MRI single-subject brain. Neuroimage. 15:273–289.
Vincent JL, Snyder AZ, Fox MD, Shannon BJ, Andrews JR, Raichle ME, Buckner RL. 2006. Coherent spontaneous activity identifies a hippocampal-parietal memory network. J Neurophysiol. 96:3517–3531.
Vogt BA, Vogt L, Laureys S. 2006. Cytology and functionally correlated circuits of human posterior cingulate areas. NeuroImage. 29:452–466.
Wang J, Aguirre GK, Kimberg DY, Roc AC, Li L, Detre JA. 2003. Arterial spin labeling perfusion fMRI with very low task frequency. Magn Reson Med. 49:796–802.
Wang J, Zhang Y, Wolf RL, Roc AC, Alsop DC, Detre JA. 2005. Amplitude-modulated continuous arterial spin-labeling 3.0-T perfusion MR imaging with a single coil: feasibility study. Radiology. 235:218–228.
Wenzel R, Bartenstein P, Dieterich M, Danek A, Weindl A, Minoshima S, Ziegler S, Schwaiger M, Brandt T. 1996. Deactivation of human visual cortex during involuntary ocular oscillations. A PET activation study. Brain. 119(Pt 1):101–110.
Wong EC, Buxton RB, Frank RL. 1998. A theoretical and experimental comparison of continuous and pulsed arterial spin labeling techniques for quantitative perfusion imaging. Magn Reson Med. 40:348–355.
Xu G, Rowley HA, Wu G, Alsop DC, Shankaranarayanan A, Dowling M, Christian BT, Oakes TR, Johnson SC. 2010. Reliability and precision of pseudo-continuous arterial spin labeling perfusion MRI on 3.0 T and comparison with 15O-water PET in elderly subjects at risk for Alzheimer's disease. NMR Biomed. 23:286–293.
Ye FQ, Berman KF, Ellmore T, Esposito G, van Horn JD, Yang Y, Duyn J, Smith AM, Frank JA, Weinberger DR, et al. 2000. H(2)(15)O PET validation of steady-state arterial spin tagging cerebral blood flow measurements in humans. Magn Reson Med. 44:450–456.
Zhang Y, Brady M, Smith S. 2001. Segmentation of brain MR images through a hidden Markov random field model and the expectation maximization algorithm. IEEE Trans Med Imaging. 20:45–57.
Zou Q, Wu CW, Stein EA, Zang Y, Yang Y. 2009. Static and dynamic characteristics of cerebral blood flow during the resting state. Neuroimage. 48:515–524.